Comparison of Aerodynamic Data Obtained by Static and Dynamic Techniques

Kenneth F. Stetson* and Frank M. Sawyer†
Air Force Flight Dynamics Laboratory, Wright-Patterson Air Force Base, Ohio

Nomenclature

A = cone base area
C_m = pitching moment coefficient, pitching moement/$q_\infty AL$, referred to a moment center at $X_{CG} = 0.65\,L$
C_N = normal force coefficient, normal force/$q_\infty A$
θ_0 = release amplitude or amplitude at midpoint of each cycle
θ_s = sting pitch angle
θ_T = model trim angle, measured from sting
ϕ = phase angle
ω = circular frequency
$(\,)_t$ = wind-off, vacuum tare run
$(\,)_w$ = wind-on run

Introduction

THE conventional internal strain gage balance system has been a standard tool for wind tunnel aerodynamics for many years. Although widely used to obtain static aerodynamic data, experimentalists have been well aware of the difficulties in obtaining accurate force and moment data at small angles of attack and of the inaccuracies which result from differentiating experimental moment data to obtain static stability derivatives. Free oscillation techniques have likewise been widely used to obtain dynamic stability data. Although persons familar with dynamic testing techniques are certainly cognizant, the technical community in general may not be aware that static aerodynamic data can readily be obtained from dynamic tests.

The purpose of this paper is to make a comparison of static aerodynamic data obtained with an internal strain gage balance and a small amplitude, free oscillation technique. Normal force coefficients, pitching moment coefficients, static stability derivatives, and center of pressure locations are compared for a biconic configuration with a 15% spherically blunted nose. Also included are the results of numerical calculations, using a shock capturing code developed by Solomon.[1]

Experimental Tests and Procedures

Two test programs were conducted independently, with the first author performing the static testing[2] and the second author the dynamic testing,[3] and the collaboration for the comparison made after each had completed his data reduction. Both test programs were performed in the AFFDL 20-in. hypersonic wind tunnel. This is a free jet, blowdown facility operated at a Mach number of 14.3 and a freestream unit Reynolds number of approximately 1.97×10^6 m^{-1} (0.6×10^6 ft^{-1}).

Received June 20, 1977; presented as Paper 77-690 at the AIAA 10th Fluid and Plasmadynamics Conference, Albuquerque, N. Mex., June 27-29, 1977; revision received Aug. 3, 1978.

Index categories: Supersonic and Hypersonic Flow; Research Facilities and Instrumentation.

*Aerospace Engineer, High Speed Aero Performance Branch, Aeromechanics Division. Associate Fellow AIAA.

†Aerospace Engineer, Control Criteria Branch, Flight Control Division.

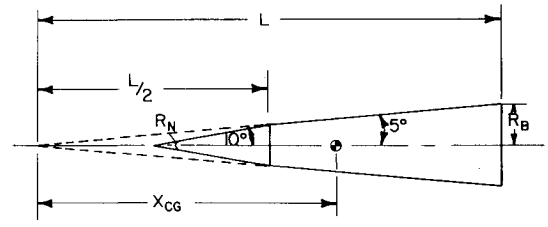

Fig. 1 Model configuration, $X_{CG} = 0.65\,L$.

A static model and a dynamic model of the same configuration and of the same size were used [$R_B = 3.81$ cm (1.5 in.)]. Figure 1 is a sketch of the model configuration. The afterbody was a truncated, 5-deg half angle, circular cone. The forebody was a 10-deg half angle, circular cone with a 15% spherically blunted tip. The model base diameter to sting diameter ratio was 3 and the sting length to model base diameter ratio was 4. These ratios have been found adequate for minimization of sting interference effects in this wind tunnel. The maximum wind-on displacement of the sting with the model oscillating was less than 0.0051 cm (0.002 in.).

The static tests were performed with a Task Corporation six-component internal strain gage balance. The design loads are shown in Table 1. Uncertainties in the balance data, based on 95% confidence limits, are also shown in the table.

Static stability derivatives C_{m_α} were obtained by measuring the slopes of a curve drawn through the C_m vs α data. The center of pressure was obtained from the relationship

$$\frac{X_{CP}}{L} = \frac{X_{CG}}{L} - \frac{C_m}{C_N} \tag{1}$$

The dynamic data were obtained by the small amplitude, free oscillation technique.[4] Typically, the oscillation amplitudes were from 1.2 to 0.7 deg. The angular displacements were recorded at 0.002 s intervals, and approximately 24 angular displacements were recorded for each cycle of oscillation.

The solution of the wind-on and wind-off linearized differential equations of motion for a one-degree-of-freedom small amplitude oscillation in pitch gives the derivative of the pitching moment coefficients as[4]

$$C_{m_\alpha} = -\frac{k}{q_\infty AL}\left[\left(\frac{\omega_w}{\omega_t}\right)^2 - 1\right] \tag{2}$$

and the time history of the motion is given by

$$\theta = \theta_T + \theta_0 e^{\lambda t}\cos(\omega t + \phi) \tag{3}$$

where θ is the angular displacement in the pitch plane measured from the pitch attitude of the sting θ_s. The trim angle θ_T is due to the static aerodynamic pitching moment at the angle of attack α. The term $\theta_0 e^{\lambda t}\cos(\omega t + \phi)$ is the damped oscillatory angular displacement about the trim.

A least-squares fit to the angular data was made, using Eq. (3). The data were section fitted, one cycle at a time, about the mean time of the section.[5] From this fitting procedure,

Table 1 Design loads

	Rated load	Uncertainty[a]
Normal force, lb	25 (each element)	±.04
Side force, lb	15 (each element)	±.03
Axial force, lb	25 (total)	±.03
Pitching moemnt, in.-lb	75 (at zero normal force)	±.07
Yawing moment, in.-lb	37.5 (at zero side force)	±.06
Rolling moment, in.-lb	100 (total)	—

[a] Based upon the calibration of this investigation.

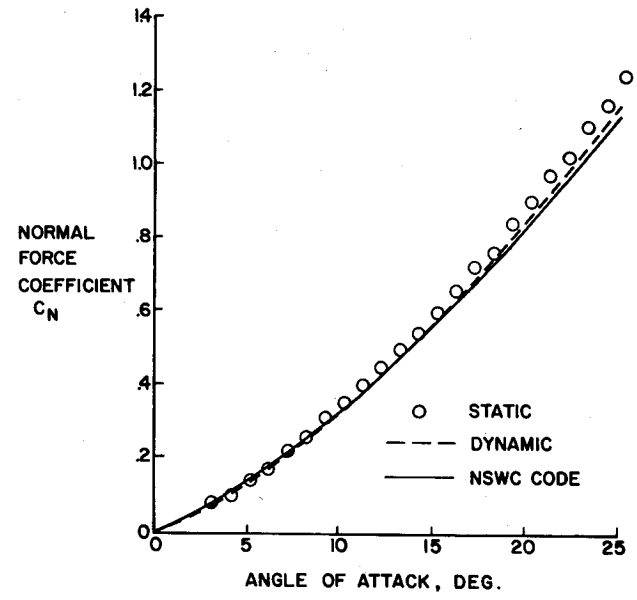

Fig. 2 Normal force coefficient vs angle of attack.

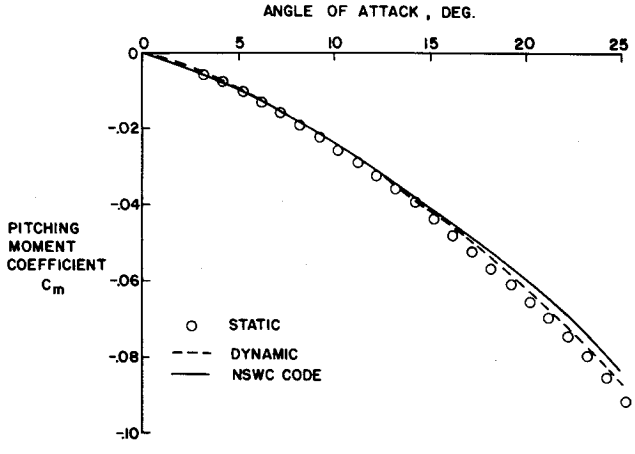

Fig. 3 Pitching moment coefficient vs angle of attack, $X_{CG} = 0.65\ L$.

oscillation amplitude, frequency, and trim angle were obtained as functions of time.

The static stability derivative C_{m_α} was then computed for each angle of attack, $\alpha = \theta_S + \theta_T$. To determine the misalignment between the model centerline and the tunnel flow, C_{m_α} was obtained at 1 deg intervals in the range $-2 < \alpha < 2$ deg. From a plot of these data, the misalignment correction was determined (typically about 0.2 deg) and this was used to correct the data. The pitching moment coefficient C_m was obtained by graphically integrating the corrected C_{m_α} vs α data.

The slope of the normal force coefficient is

$$C_{N_\alpha} = \frac{C^*_{m_\alpha} - C_{m_\alpha}}{\Delta X/L} \tag{4}$$

where the derivatives C_{m_α} and $C^*_{m_\alpha}$ are obtained from two sets of free oscillation tests with the pivot located at two different axial stations, $X_{CG} = 0.65\ L$ and $X_{CG} + \Delta X = 0.75\ L$, respectively. Integrating C_{N_α} then gives the normal force coefficient C_N. The center of pressure, with the moment center at 0.65 L, is obtained from Eq. 1. At $\alpha = 0$, C_{m_α} and C_{N_α} are substituted for C_m and C_N when determining X_{CP}.

Results and Discussion

Figures 2-5 compare the data obtained by the two experimental techniques. Also shown are results obtained by a

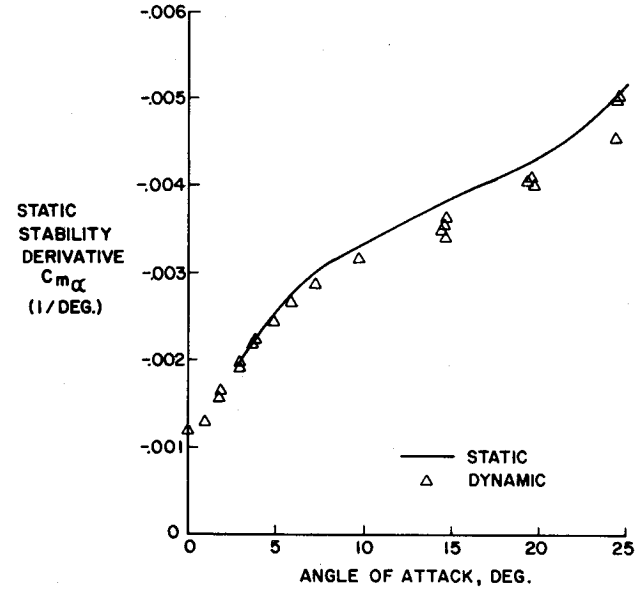

Fig. 4 Static stability derivative vs angle of attack, $X_{CG} = 0.65\ L$.

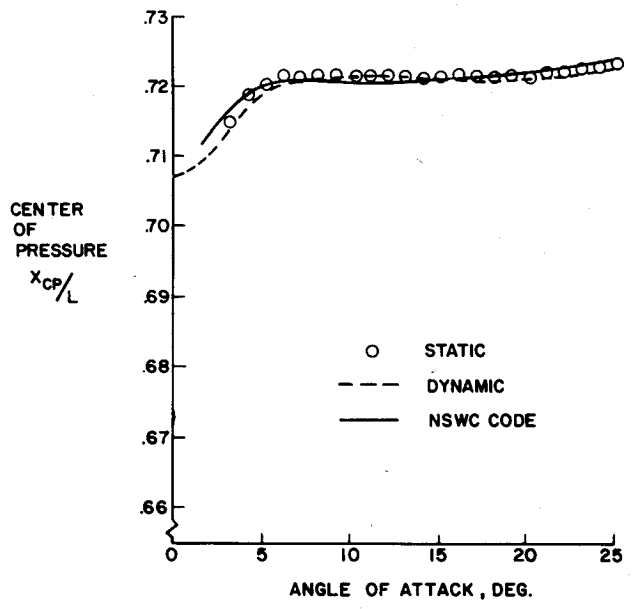

Fig. 5 Center of pressure vs angle of attack.

shock capturing computer code recently developed by Solomon.[1] When comparing normal force coefficients (Fig. 2) and pitching moment coefficients (Fig. 3) close agreement was found between static and dynamic data. The dynamic data were consistently lower than the static data, with differences generally between 2 and 5%. The numerical results were in good agreement with the experimental data at low angles of attack. Small differences occurred at angles of attack larger than about 15 deg. Figure 4 shows the data comparison for the static stability derivative C_{m_α}. Note that C_{m_α} vs α is nonlinear, even at small angles of attack. Figure 5 compares the center of pressure locations obtained by the two experimental techniques and Solomon's code. The experimental and inviscid numerical results are seen to agree very closely. Such good agreement, by three independent techniques, promotes confidence in the results of each technique.

Estimates of the uncertainty in the determination of the centers of pressure are shown in Fig. 6. These estimates, for 95% confidence limits, are based on calibration uncertainties of the data system for each technique. Misalignment between

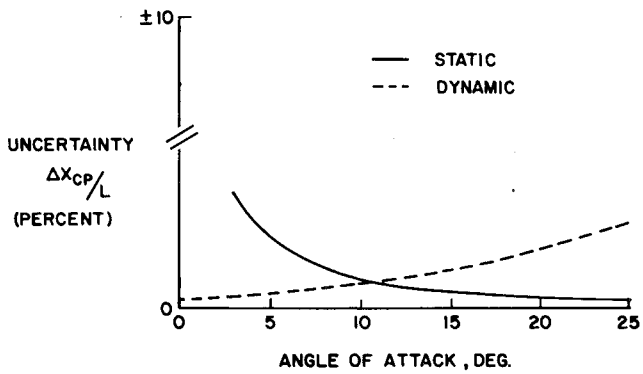

Fig. 6 Uncertainty in center of pressure vs angle of attack.

the model centerline and the tunnel flow at $\alpha = 0$ was not considered. Also, since the tests were conducted in the same facility with models of the same size, tunnel calibration uncertainties and flow conditions peculiar to this wind tunnel were not included in the uncertainty estimates. The intent here was only to illustrate the relative values and trends for the two techniques used. The uncertainty in X_{CP}/L for the static measurements increases with decreasing angle of attack. Since this characteristic depends primarily upon the balance calibration uncertainties, smaller uncertainty in the measurement of X_{CP}/L could be obtained by using a more sensitive balance. For example, this approach was used recently by Adams and Griffith,[6] who used a special force balance to investigate static stability characteristics of a sharp 5 deg cone at angles of attack up to 4 deg. For the dynamic measurements, the uncertainty in X_{CP}/L is least at $\alpha = 0$ and increases gradually with increasing angle of attack. This increase in uncertainty is possibly due to unsteady flowfield effects. The increasing "noise" observed in the θ vs t plots for the larger angles of attack supports this speculation.

In deciding which experimental technique to use to obtain static aerodynamic data, the primary consideration must be the purpose of the test. If accurate results in the small angle of attack range are not required, then a general purpose force balance is the better choice. If the emphasis is in the low angle of attack regime one has the option of using the dynamic testing technique or using a special, very sensitive, force balance. It should be noted that the damping derivatives are also obtained from the dynamic tests.[3,4]

The static balance is relatively simple to use, allows rapid data reduction, and yields data of low uncertainty for moderate to large angles of attack. Dynamic testing is more intricate and data reduction is more involved and time consuming; however, this technique provides a method of obtaining static data with low uncertainty at small angles of attack, including $\alpha = 0$.

References

[1] Solomon, J. M., Ciment, M., Ferguson, R. E., and Bell, J. B., "Inviscid Flow Field Calculations for Re-entry Vehicles with Control Surfaces," *AIAA Journal*, Vol. 15, Dec. 1977, pp. 1742-1749.

[2] Stetson, K. F., and Lewis, A. B., "Aerodynamic Comparison of a Conical and Biconic Reentry Vehicle," AIAA Paper 77-1161, Aug. 1977.

[3] Sawyer, F. M., "Wind Tunnel Tests at Mach 14 on a Slender Biconic Reentry Vehicle with Various Nose Bluntness," AFFDL/FGC TM 76-52, Air Force Flight Dynamics Laboratory, April 1976.

[4] Walchner, O., Sawyer, F. M., and Koob, S. J., "Dynamics Stability Testing in a Mach 14 Blowdown Wind Tunnel," ARL 64-221, AD 454 735, Aerospace Research Laboratories, 1964; also, *Journal of Spacecraft and Rockets*, Vol. 1, July-August 1964, pp. 437-439.

[5] Eikenberry, R. S., "Analysis of Angular Motion of Missiles," Sandia Laboratories SC-CR-70-6051, Feb. 1970.

[6] Adams, J. C., Jr. and Griffith, B. J., "Hypersonic Viscous Static Stability of a Sharp 5-deg Cone at Incidence," *AIAA Journal*, Vol. 14, Aug. 1976, pp. 1062-1068.

Flat Plate Turbulent Boundary Layers Subject to Large Pressure Fluctuations

S. Raghunathan* and J. B. Coll†
The Queen's University of Belfast, Belfast, N. Ireland
and
D. G. Mabey‡
Royal Aircraft Establishment, Bedford, England

Nomenclature

C_f = skin friction coefficient $= \tau_w / q$
e = hot wire output voltage
f = frequency, Hz
$F(n)$ = contribution to $\bar{p}^2/q^2$ in frequency band Δn
$\sqrt{nF(n)}$ $= p/q(\epsilon)^{1/2}$
M = Mach number
n = frequency parameter $= fw/U$
p = pressure
q = freestream kinetic pressure $= \frac{1}{2}\rho U^2$
R = Reynolds number based on wire diameter $= Ud/\nu$
R_θ = momentum thickness Reynolds number $= U\theta/\nu$
r = overheat parameter
$S_\rho, S_u, S_{T_0}, S_{\rho u}$ = hot wire sensitivity to density, velocity, total temperature, and mass flow fluctuations
T_0 = total temperature
U = freestream velocity
u = local velocity
w = width of tunnel
x = distance from the start of the slot(s)
ρu = mass flow
β = pressure gradient parameter $= \delta^* \dfrac{dp/dx}{\tau_w}$
δ = boundary-layer thickness at $u = 0.99U$
δ^* = boundary-layer displacement thickness

$$= \int_0^\infty \left(1 - \frac{\rho u}{\rho_1 U_1}\right) dy$$

θ = boundary-layer momentum thickness

$$= \int_0^\infty \frac{\rho u}{\rho_1 U_1}\left(1 - \frac{\rho u}{\rho_1 U_1}\right) dy$$

ϵ = analyzer bandwidth ratio $= \Delta f/f$
ρ = density
τ_w = wall shear stress
ν = kinematic viscosity

Superscripts

$( )'$ = instantaneous values of the fluctuating quantities
$(\bar{\ })$ = root mean square value of the fluctuating quantities

Subscript

1 = freestream value

Received May 31, 1978; revision received Sept. 8, 1978.

Index categories: Boundary Layers and Convective Heat Transfer—Turbulent; Subsonic Flow; Transonic Flow.

*Lecturer, Dept. of Aeronautical Engineering.
†Research Assistant. Member AIAA.
‡Principal Scientific Officer, Structures Dept.